J Eng Math (2011) 69:71–90
DOI 10.1007/s10665-010-9378-8

A thermal elastic model for constrained crystal growth with facets

Jinbiao Wu · C. Sean Bohun · Huaxiong Huang

Received: 2 July 2009 / Accepted: 4 May 2010 / Published online: 23 May 2010

Abstract A model for computing thermal stress inside a crystal with facets is presented. Using a systematical perturbation analysis, a semi-analytical thermal-stress solution is obtained for constrained directional growth with small lateral heat flux. This solution can be applied to crystals grown by various growth techniques such as the Czochralski method. The semi-analytical nature of the solution leads to a much more efficient approach for computing thermal stress in crystals with facets, compared to a full 3D simulation. Examples are given for crystals pulled in a variety of seed orientations.

Keywords Geometric anisotropy · Asymptotic expansion · Czochralski technique · Facet formation · Finite-difference method · Thermal stress

1 Introduction

Directional growth techniques such as the Czochralski (Cz) method are frequently used to produce high-quality single crystals. Almost perfectly cylindrical crystals are grown for silicon and other semiconductor materials despite their internal structure and material anisotropy. For these crystals, the effect of material anisotropy on thermal stress has been investigated by assuming axisymmetric cylindrical shape [1–4]. On the other hand, anisotropic effects such as facets are often visible on the surface of binary compound semiconductor crystals grown by these methods [5,Chap. 5]. The effect of non-cylindrical shape on the thermal stress is therefore of practical interest.

In this paper, we extend a thermal-stress model developed in [6] for axisymmetric crystals to geometrically anisotropic ones grown by directional growth techniques. Under the assumptions of weak lateral heat flux and anisotropic

J. Wu
School of Mathematical Sciences, Peking University, Beijing 100871, China
e-mail: jwu@math.pku.edu.cn

C. S. Bohun
Faculty of Science, University of Ontario Institute of Technology, Oshawa, ON L1H 7K4, Canada
e-mail: sean.bohun@uoit.ca

H. Huang (✉)
Department of Mathematics and Statistics, York University, Toronto, ON M3J 1P3, Canada
e-mail: hhuang@yorku.ca

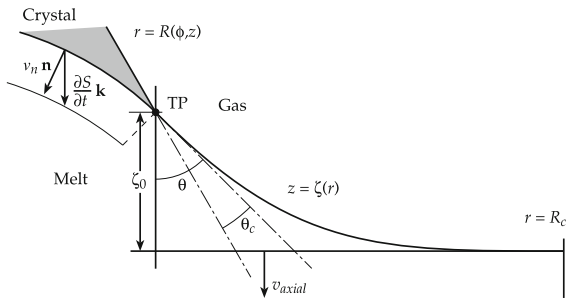

Fig. 1 Schematic diagram of the meniscus $z = \zeta(r)$ with capillary height ζ_0, defined on $R(S) \le r \le R_c$, where $R(S)$ is the radius of the crystal at the interface, θ_c is the contact angle, and R_c is the radius of the crucible. The motion of the triple point (TP) is determined by the advancing interface S, and the axial growth rate v_{axial} which incorporates both the pull rate applied to the crucible and the speed at which the melt falls. In practice, both the seed is lifted and the crucible holding the melt is dropped

effects, we derive perturbation solutions for temperature and related thermal stress. As in [6], weak lateral heat flux is characterized by a small Biot number, which allows us to expand the temperature into an asymptotic series and reduce a three-dimensional problem to a series of two-dimensional ones. When the anisotropic effect is weak, we can further convert these two-dimensional problems into a series of one-dimensional (axisymmetric) ones. Similar expansions can be carried out for the thermal stress and an explicit solution can be obtained, based on one-dimensional temperature solutions. As a result, the thermal stress can be computed without solving the thermal elastic equations which are originally three-dimensional in space. As in [6] and previous studies in the literature, the thermal elastic stress is used as an indicator in this paper for predicting the formation of grown-in defects (dislocations) inside the crystals. The focus here is to investigate the additional effect on thermal stress due to the formation of facets.

To incorporate geometrical anisotropy into existing thermal-stress models [3, 6], we need to predict facet formation and lateral crystal shape under growth constraints imposed by directional growth. While a significant amount of research on shape predictions has been carried out and documented in the literature (see [7] and references therein), much less attention has been paid to facet formation using directional growth techniques. For directional growth, typically the lateral growth rate is given by

$$v_{\text{lateral}} = v_{\text{axial}} \tan(\theta - \theta_c), \tag{1}$$

where v_{axial} is the axial growth rate (rate of crystallization), θ is the angle between the meniscus and the axial direction, and θ_c is the contact angle between the crystal and the melt. Details of the geometry can be found in Fig. 1. In [8], a phenomenological model has been used for the contact angle

$$\theta_c = \bar{\theta}_c\,[1 + \alpha \cos(k\phi)], \tag{2}$$

where $\bar{\theta}_c$ is the mean contact angle, ϕ is the angle formed by the normal direction of the growth front and an intrinsic direction determined by the crystal structure, k is an integer, which is chosen in such a way as to reflect a certain symmetry (e.g., $k = 4$ for a cubic lattice structure), and α is a parameter representing the degree of anisotropy. For unconstrained growth, these types of models are commonly used to study pattern selection, morphological instability [9,Chap. 5], [10, 11] as well as the growth of poly-crystals [7].

The model in [8] is useful when the primary interest is on facet formation of crystals grown by directional growth techniques. However, we must make a priori assumptions about the nature of the symmetry in the contact angle (based on surface energy). It is not clear how to estimate the relevant coefficients in those models in a way that is not only consistent with the material anisotropy but also faithful to the complex interaction between the orientation of the crystal and its underlying lattice structure. In this paper, we propose a simple model for the lateral growth rate, which takes the following form

$$v_{\text{lateral}} = v_{\text{axial}} \min\{f(\mathbf{n} \cdot \mathbf{e}), \tan(\theta - \bar{\theta}_c)\}, \tag{3}$$

where $f(\cdot)$ is a given function of the angle formed by the normal direction of the lateral surface in the horizontal plane ($\mathbf{n}$) and a reference direction ($\mathbf{e}$). The characteristic function $f(\cdot)$ is determined only by the lattice structure and

pulling direction and is therefore consistent with the material anisotropy of the crystal. In other words, we assume that the ratio of the growth rate is determined by the crystal-lattice structure unless the constraint for directional growth is active. More details on the construction of f can be found in the Appendix.

Using our growth model, we could predict facet formation and shape evolution during the entire growth process, starting from an arbitrary seed shape in any crystallographic orientation. Indeed, a perturbation solution for thermal stress is obtained following the growth model given by (3). However, computational results are only presented for idealized growth conditions where we fix the growth angle and assume an equilibrium lateral crystal shape, predicted by our model. This is due to the fact that our main objective of this paper is to investigate the effect of geometric anisotropy on thermal stress instead of an exhaustive study on shape evolution and facet formation using directional growth techniques.

The effect of anisotropy appears in two aspects: a geometric effect due to facet formation, and an intrinsic effect due to the anisotropy in the material (elastic) parameters of the crystal. In this paper we investigate the geometric effect while the material anisotropy case is considered in [12]. In Sect. 2 we will present a mathematical model for lateral growth and the thermal problem is described in Sect. 3. A perturbation solution for temperature is obtained in Sect. 4. In Sect. 5, we derive an expression for the thermal stress using isotropic elastic constants. Numerical results are presented in Sect. 6 for the [001], $[\bar{1}\bar{1}\bar{1}]$ and $[\bar{2}11]$ pulling directions[1] in the growth of a crystal with cubic symmetry. We conclude the paper by summarizing our results and briefly discussing future directions of research.

2 Constrained lateral growth and facet formation

Before one can determine the shape of a given crystal, one first needs to compute the growth rate as a function of the crystal orientation. Studies based solely on the crystal-lattice geometry using the BFDH law and PBC energy methods [13] neither make consideration of the bond types nor explain the different growth rates between the positive and negative directions in a polar crystal such as the III–V semiconductors [14].

In order to include the polarity effects, Zhong et al. [15, 16] suggested a coordination polyhedral growth unit model where the growth of the various crystal faces is related to the exposure of edges, angle, and planes of the anion-coordination polyhedra on these surfaces. The idea of representing the crystal structure in this manner predates the work of Zhong [17–21]. What is more recent is the concept of attributing the growth rate of a given crystal with the incorporation of these complexes rather than the incorporation of individual atoms. This idea has continued to develop in a series of recent papers [14, 22–26].

The important characteristic of the coordination polyhedra is that the element (face, edge, vertex) exposed at a given interface depends on its orientation. In this sense the growth rates of the various crystal faces are related to the element of the coordination polyhedron present at the interface. Quantitative growth rates can be obtained by noting that, if a given polyhedra is an equilibrium shape, the growth rate in any direction must be proportional to the thickness of a single shell of growth units added in that direction. This simple idea can be generalized to other coordination polyhedra and it reflects the vertex, edge, face hierarchy noted above.

If we let AB denote a III–V semiconductor that belongs to the zinc-blende class of crystals, then its anion-coordination polyhedra are the AB_4^{6-} tetrahedrons illustrated in Fig. 2. By expressing the unit cell in terms of the tetrahedral growth units, the polarities of the III–V compounds naturally arise. The [111] (head) direction consists of exposed vertices and a fast growth rate, whereas the $[\bar{1}\bar{1}\bar{1}]$ (tail) direction consists of exposed faces and a slow growth rate.

If one considers Cz growth, then the growth of the crystal is constrained to only those directions into the melt, and laterally, due to the meniscus supported at the crystal/melt interface. Indeed, to grow a cone with a $1/2$ growing angle of φ, we require

$$\tan\varphi = \frac{v_{\text{lateral}}(\mathbf{n})}{v_{\text{axial}}},$$

[1] $[h\bar{k}l]$ denotes a unit vector in the $\langle h, -k, l\rangle$ direction.

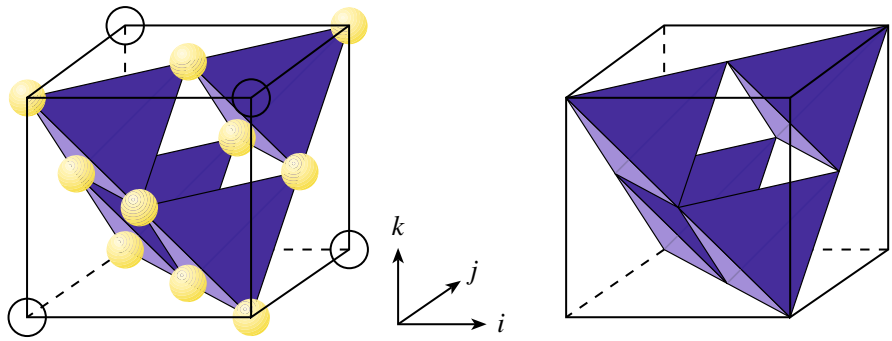

Fig. 2 Shown are the four tetrahedra of an AB unit cell. To the *left* only the B atoms in the unit cell are shown. B atoms in the unit cell but not included in the four growth units are represented with *hollow circles*. At the centre of each tetrahedral growth unit is an A atom accounting for all the atoms in the AB unit cell. On the *right* only the tetrahedra are shown

where $\mathbf{n}$ denotes the lateral growth direction. However, since $v_{\text{lateral}}(\mathbf{n})$ depends on the lateral direction, those directions where $\tan^{-1}(v_{\text{lateral}}(\mathbf{n})/v_{\text{axial}}) \geq \varphi$ cannot be supported by the meniscus and will be truncated. Similarly, directions where $\tan^{-1}(v_{\text{lateral}}(\mathbf{n})/v_{\text{axial}}) < \varphi$ will correspond to possible facets in the lateral direction. Following this, the growth angle $\psi(\mathbf{n})$ is given by

$$\psi(\mathbf{n}) = \min\left\{\varphi,\ \tan^{-1}\left(\frac{v_{\text{lateral}}(\mathbf{n})}{v_{\text{axial}}}\right)\right\}.$$

Starting with a circular seed, we evolve a two-dimensional cross-section corresponding to a lateral growth profile, $v_{\text{lateral}}(\mathbf{n})$, for a given pulling direction. The axial growth is in the opposite direction that the crystal is pulled and defines $\psi(\mathbf{n})$.

For the three characteristic directions [001], $[\bar{1}\bar{1}\bar{1}]$ and $[\bar{2}11]$, Fig. 3 shows the constrained relative growth angle $\psi(\mathbf{n})$ and the resulting equilibrium cross-sections (ECS) for a conic crystal grown with a 1/2 opening angle of $\varphi_{\text{cone}} = 5°$. A representation of the ECS according to expression (5a) is tabulated in Table 1.

3 Thermal problem

We first describe the thermal problem in detail. The temperature inside the crystal is governed by the heat equation while the domain is varying with time as the crystal is being pulled out of the melt. The basic assumptions of our model are that the lateral heat flux is small and the material and geometric anisotropic effects are weak. To simplify the discussion, we will assume that lateral heat transfer from the crystal to the background is known. In principle, we could incorporate the effect of the melt flow by coupling the heat-transfer process in the crystal with that in the melt. However, to concentrate on the thermal stress in the crystal, we will neglect the effect of the melt flow and assume that the axial heat flux from the melt at the crystal/melt interface does not vary in the cross-sectional (radial and circumferential) directions.

As depicted in Fig. 4, within the crystal $\Omega(t)$, defined by $r \leq R(z, \phi)$ and $0 \leq z \leq S(r, \phi, t)$, the solidification front, the temperature $T(\mathbf{x}, t)$ satisfies the heat equation,

$$\rho_s c_s \frac{\partial T}{\partial t} = \nabla \cdot (k_s \nabla T), \quad \mathbf{x} \in \Omega(t), \tag{4a}$$

where ρ_s, c_s and k_s are the density, specific heat, and thermal conductivity of the crystal. The boundary conditions are as follows:

$$-k_s \frac{\partial T}{\partial \mathbf{n}} = h_{\text{gs}}(T - T_g) + h_F(T^4 - T_b^4), \quad \mathbf{x} \in \Gamma_g, \tag{4b}$$

$$k_s \frac{\partial T}{\partial z} = h_{\text{ch}}(T - T_{\text{ch}}), \quad z = 0, \tag{4c}$$

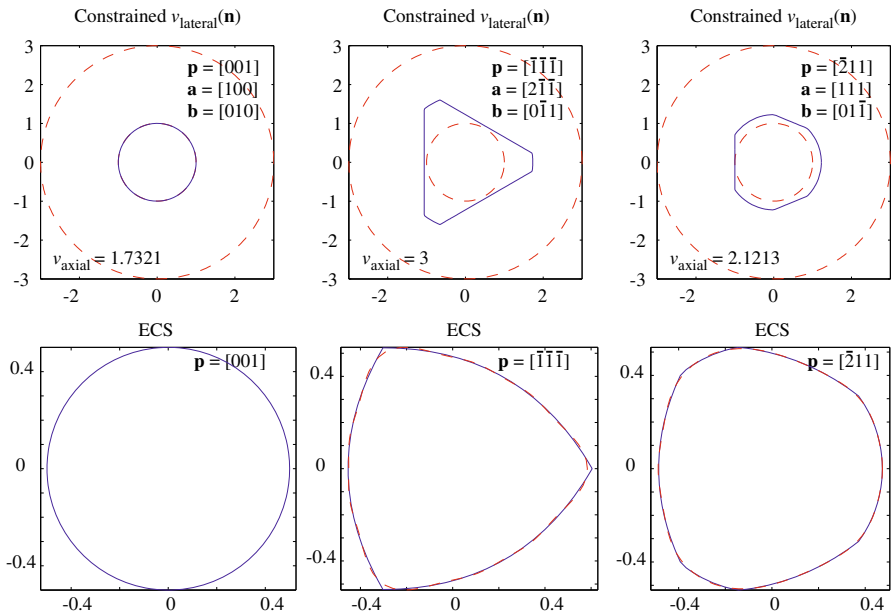

Fig. 3 Shown are the relative lateral growth rates $v_{\text{axial}} \tan\psi(\mathbf{n})$ where $\tan\psi(\mathbf{n}) = \min\{v_{\text{lateral}}(\mathbf{n})/v_{\text{axial}}, \tan\varphi\}$ and equilibrium cross-sections for the pulling directions $\mathbf{p} = [001]$, $[\bar{1}\bar{1}\bar{1}]$ and $[\bar{2}11]$. The vector $-\mathbf{p}$ is directed into the melt and has the growth rate v_{axial}. $\mathbf{a}$ and $\mathbf{b}$ correspond to $\phi = 0$ and $\phi = \pi/2$, respectively. The curves $r = 1$ and $r = 3$ in plots of v_{lateral}, respectively, correspond to the growth rate in the face and vertex directions of the underlying growth units. In the simulation the contact angle is taken to be 25° corresponding to the III–V material InSb. The crystal is constrained to grow into a cone with a 1/2 opening angle of $\varphi_{\text{cone}} = 5°$. Where discernible, the *dashed curve* in the ECS plots correspond to the data in Table 1. We note that our model produces crystals with shapes similar to those grown by our industrial partner [5,Chap. 5]

Table 1 Parameters corresponding to expression (5a) for the equilibrium cross-sections illustrated in Fig. 3

In all cases $n_k = k$, $m = 10$ and $\delta_k = 0$. The results are obtained by starting with a circular seed with 1200 facets and computing an FFT on the final shape with $N = 262144$ points

k	$\beta_k : \mathbf{p} = [001]$ $\alpha = 0.00083$	$\beta_k : \mathbf{p} = [\bar{1}\bar{1}\bar{1}]$ $\alpha = 0.12313$	$\beta_k : \mathbf{p} = [\bar{2}11]$ $\alpha = 0.08918$
1	1.00000	0.00003	−0.66503
2	0.00023	0.00004	−0.22615
3	0.00002	0.95149	0.63239
4	0.00002	0.00001	−0.29841
5	0.00002	0.00002	−0.11419
6	0.00002	0.27930	0.02665
7	0.00002	0.00001	−0.03487
8	0.00002	0.00002	0.04491
9	0.00002	0.12903	−0.00703
10	0.00002	0.00001	0.02444

where h_{gs} and h_{ch} represent the heat-transfer coefficients; h_F the radiation heat-transfer coefficient; T_g, T_{ch} and T_b denote the ambient gas temperature, the chuck temperature and background temperature, respectively. The growth of the domain $\Omega(t)$ is due to the solidification. It consists of the axial growth governed by the Stefan condition, given below, and the lateral growth discussed in the previous section. In general, the domain $\Omega(t)$ cannot be determined a priori to the temperature solution since it consists of free boundaries, and the growth mechanism is coupled with temperature and depends on the crystal structure. One of the main objectives of this paper is to show that, under certain conditions, approximation to $\Omega(t)$ can be used to simplify the calculations.

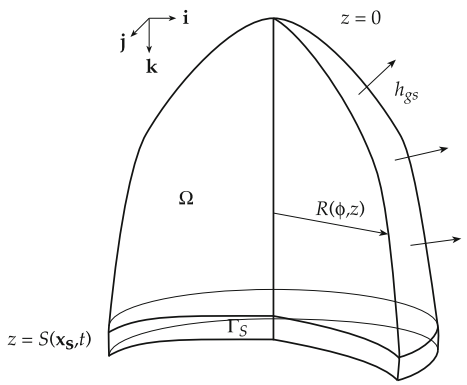

Fig. 4 Shown is a typical crystal at some time t during a growth run with a newly solidified portion at $z = S(\mathbf{x_s}, t)$. The coordinate system is chosen so that the top of the crystal remains at $z = 0$ and the solidification front grows downward in the positive z-direction. The radial profile is given by $R(\phi, z)$ and the crystal length is $S(\mathbf{x_s}, t)$. Finally, the heat-transfer coefficient h_{gs} may be a function of the axial position z. Omitted for clarity is the seed and chuck which extracts the crystal from the melt

The crystal/melt interface is denoted Γ_S and is where

$$T = T_m, \tag{4d}$$

the melting temperature. Explicitly we denote the melting isotherm by $z - S(\mathbf{x_s}, t) = 0$, for $\mathbf{x_s} \in \Gamma_S$. The motion of the interface of the phase transition is governed by the Stefan condition

$$\rho_s L|\mathbf{v}_n| = k_s \left.\frac{\partial T}{\partial \mathbf{n}}\right|_{z\to S^-} - q_{l,n}, \quad |\mathbf{v}_n| = v_n = \frac{\partial S}{\partial t}\mathbf{k}\cdot\mathbf{n} \tag{4e}$$

where L is the latent heat, $|\mathbf{v}_n|$ is the speed of the interface in the direction of its outward normal $\mathbf{n}$, and $q_{l,n}$ is the heat flux from the melt normal to the interface. The speed $\partial S/\partial t$ is the speed of the interface S in the $\mathbf{k}$ direction (see Fig. 1).

3.1 Crystal shape

For the purpose of computing the thermal stress, we assume the following expression in the case of weak anisotropy (α small)

$$R(\phi, z) = \bar{R}(z)\left(1 + \alpha \sum_{k=1}^{m} \beta_k \cos\left(n_k\phi + \delta_k\right)\right) = \bar{R}(z)\left(1 + \alpha\lambda(\phi)\right), \tag{5a}$$

where a cylindrical coordinate system is chosen for convenience. In this expression $2\pi\bar{R}(z) = \int_{-\pi}^{\pi} R(\phi, z)\,\mathrm{d}\phi$; $m, n_1 < n_2 < \cdots < n_m$ are positive integers ($m = 1, n_1 = 4$ for four-fold symmetry); the $\delta_k \in [0, 2\pi)$ are chosen to ensure that $\beta_k > 0$. Note that only those n_k corresponding to $\beta_k > 0$ are represented in the series. The parameter $\alpha \geq 0$ is a measure of the geometric anisotropy and choosing the β_k so that $\sum_{k=1}^{m} \beta_k^2 = 1$ yields the expression

$$\alpha^2 = \frac{1}{\pi\bar{R}(z)^2} \int_{-\pi}^{\pi} \left(R(\phi, z) - \bar{R}(z)\right)^2 \mathrm{d}\phi. \tag{5b}$$

We will assume that $\alpha < 1$ which will certainly[2] be the case if $\max_\phi R(\phi, z) < \frac{3}{2}\bar{R}(z)$. The enclosed area and circumference of R at any value of z satisfy $A(z) = \bar{R}^2 I_{2,0}/2$ and $s(z) = \bar{R} I_{0,1}$ respectively where

$$I_{i,j} = \int_0^{2\pi} (1 + \epsilon\lambda)^i \left((1 + \epsilon\lambda)^2 + (\epsilon\lambda')^2\right)^{j/2} \mathrm{d}\phi, \quad \lambda' = \frac{\mathrm{d}\lambda}{\mathrm{d}\phi}. \tag{5c}$$

[2] This is simply a consequence of the positivity of R and the mean-value theorem applied to (5b).

We assume that the lateral shape of the crystal is in equilibrium with coefficients given in Sect. 2 for the three pulling directions being considered in this paper.

3.2 Non-dimensionalization

For simplicity, we assume that the gas temperature T_g is constant. The Biot number is defined by

$$\epsilon = \frac{\bar{h}_{\rm gs}\tilde{R}}{k_s}, \tag{6}$$

where $\tilde{R}$ is a characteristic radius of the crystal and $\bar{h}_{\rm gs}$ is the mean value of $h_{\rm gs}$. We adopt the following scalings:

$$r = \tilde{R}\hat{r}, \quad R = \tilde{R}\hat{R}, \quad \epsilon^{1/2}z = \tilde{R}\hat{z}, \quad \epsilon^{1/2}S = \tilde{R}\hat{S},$$
$$\mathrm{St} = \frac{L}{c_s\Delta T}, \quad \Delta T = T_m - T_g, \quad T = T_g + \Delta T\Theta, \quad t = \frac{\mathrm{St}\tilde{R}^2\rho_s c_s}{k_s\epsilon}\hat{t},$$

with $\phi = \hat{\phi}$. Here variables with hats ($\hat{}$) are the non-dimensional ones. In terms of these variables the heat equation (4a) becomes

$$\frac{\epsilon}{\mathrm{St}}\Theta_t = \frac{1}{r}(r\Theta_r)_r + \frac{1}{r^2}\Theta_{\phi\phi} + \epsilon\Theta_{zz}, \quad \mathbf{x} \in \Omega(t), \tag{7a}$$

with boundary conditions (4b)–(4d)

$$-\Theta_r + \frac{1}{R^2}R_\phi\Theta_\phi + \epsilon R_z\Theta_z = \epsilon F(\Theta)\left(1 + \frac{R_\phi^2}{R^2} + \epsilon R_z^2\right)^{1/2}, \quad \mathbf{x} \in \Gamma_g, \tag{7b}$$

$$\Theta_z(0,\phi,t) = \delta\left(\Theta(0,\phi,t) - \Theta_{\rm ch}\right), \tag{7c}$$

$$\Theta = 1, \quad \mathbf{x} \in \Gamma_S, \tag{7d}$$

where

$$F(\Theta) = \frac{h_F(T_g^4 - T_b^4)}{\bar{h}_{\rm gs}\Delta T} + \left(\beta + \frac{4h_F}{\bar{h}_{\rm gs}}T_g^3\right)\Theta + \frac{h_F}{\bar{h}_{\rm gs}}\Delta T(6T_g^2 + 4T_g\Delta T\Theta + \Delta T^2\Theta^2)\Theta^2,$$

$\beta = h_{\rm gs}/\bar{h}_{\rm gs}$, and $\delta = \epsilon^{1/2}h_{\rm ch}/\bar{h}_{\rm gs}$. The hats have been dropped for brevity. The crystal/melt interface advances according to the Stefan condition (4e) which in non-dimensional co-ordinates becomes

$$\Theta_z - \frac{1}{\epsilon}S_r\Theta_r - \frac{1}{\epsilon r^2}S_\phi\Theta_\phi = \gamma + S_t, \quad \gamma = \frac{q_l\tilde{R}}{\epsilon^{1/2}k_s\Delta T}, \tag{7e}$$

where γ (q_l) is the non-dimensional (dimensional) heat flux in the liquid across the crystal/melt interface in the axial direction.

Before we proceed to obtain the temperature solution, we remark that the problem considered here is superficially similar to the continuous-casting problem investigated in [27–29]. However, in the Cz method experienced by the InSb crystals, the time scale of the solidification is much longer than that with continuous casting. In addition, heat loss in the lateral direction is discouraged when attempting to grow single crystals that are free of defects. Because of this long timescale, the thermal problem decouples from the solidification problem. Therefore, the thermal field can be obtained by solving the quasi-steady equation.

4 Temperature solution

Much of the asymptotic framework discussed in this paper has appeared elsewhere in the literature [6, 30–35] in an axisymmetric case. Kuiken and Roksnoer [32] obtained an accurate temperature distribution for a Si crystal grown with the floating-zone technique. By using an expansion in terms of the Péclet and Nusselt numbers of the crystal, they obtained a solution valid for slender crystals grown in conductive heat-transfer environments. An asymptotic analysis that considered the melt was undertaken by Brattkus and Davis [30], where the geometry allowed an expansion in terms of the aspect ratio of the solidification cell. Young and Chait [33] considered a system driven by surface tension and more recently Young and Heminger [34, 35] have utilized a small aspect ratio to study the growth of single crystal fibres.

Equations 7a and 7b strongly suggest that the temperature Θ is independent of r and ϕ to leading order. If true then the crystal/melt interface S is also independent of r and ϕ to leading order. These observations motivate the following expansions:

$$\Theta \sim \Theta_0(z,t) + \epsilon\Theta_1(r,\phi,z,t) + \epsilon^2\Theta_2(r,\phi,z,t) + \cdots, \tag{8}$$
$$S \sim S_0(t) + \epsilon S_1(r,\phi,t) + \epsilon^2 S_2(r,\phi,t) + \cdots$$

within the crystal $\Omega(t)$. We substitute them into the scaled model, expand in powers of ϵ, simplify and collect terms of the same orders. The resulting field equations to first order are:

$$\frac{1}{\mathrm{St}}\Theta_{j,t} - \Theta_{j,zz} = \frac{1}{r}(r\Theta_{j+1,r})_r + \frac{1}{r^2}\Theta_{j+1,\phi\phi}, \quad \mathbf{x} \in \Omega(t), \quad j = 0, 1, \tag{9}$$

where the boundary condition on the lateral surface becomes

$$\left(\Theta_{1,r} - \frac{1}{R^2}R_\phi\Theta_{1,\phi} - R_z\Theta_{0,z} + F(\Theta_0)\left(1 + \frac{R_\phi^2}{R^2}\right)^{1/2}\right)(R,\phi,z,t) = 0, \tag{10a}$$

$$\left(\Theta_{2,r} - \frac{1}{R^2}R_\phi\Theta_{2,\phi} - R_z\Theta_{1,z} + F'(\Theta_0)\Theta_1\left(1 + \frac{R_\phi^2}{R^2}\right)^{1/2} + \frac{1}{2}R_z^2F(\Theta_0)\left(1 + \frac{R_\phi^2}{R^2}\right)^{-1/2}\right)(R,\phi,z,t) = 0. \tag{10b}$$

Continuing this procedure for the remaining conditions, at the top of the crystal one has

$$\Theta_{0,z}(0,t) = \delta(\Theta_0(0,t) - \Theta_{\mathrm{ch}}), \tag{11a}$$
$$\Theta_{1,z}(r,\phi,0,t) = \delta\Theta_1(r,\phi,0,t), \tag{11b}$$

and at the solid–liquid interface

$$\Theta_0(S_0(t),t) = 1, \tag{12a}$$
$$\left(S_1\Theta_{0,z} + \Theta_1\right)(r,S_0(t),t) = 0. \tag{12b}$$

Finally, the evolution of the interface is governed by

$$S_0'(t) = \Theta_{0,z}(S_0(t),t) - \gamma, \tag{13a}$$
$$S_{1,t}(r,\phi,t) = \left(\Theta_{1,z} + S_1\Theta_{0,zz} + \frac{\Theta_{1,r}^2}{\Theta_{0,z}} + \frac{\Theta_{1,\phi}^2}{r^2\Theta_{0,z}}\right)\Bigg|_{z=S_0(t)}, \tag{13b}$$

with initial conditions $S_0(0) = Z_0$ and $S_1(r,\phi,0) = 0$. Here Z_0 is the non-dimensional length of the seed.

4.1 Solution of the zeroth-order model

Let $\Delta_{r\phi}$ denote the two-dimensional Laplacian operator in (r, ϕ) so that (9) with $j = 0$ and (10a) can be written as

$$\Delta_{r\phi}\Theta_1 = \frac{1}{\mathrm{St}}\Theta_{0,t} - \Theta_{0,zz}, \quad \mathbf{x} \in \Omega(t), \tag{14a}$$

$$\frac{\partial \Theta_1}{\partial \mathbf{n}_{r\phi}} = -F(\Theta_0) + R_z\Theta_{0,z}\left(1 + \frac{R_\phi^2}{R^2}\right)^{-1/2}, \quad r = R(\phi, z). \tag{14b}$$

Here $\mathbf{n}_{r\phi}$ is the unit normal vector in the cross-section. A necessary condition for the existence of Θ_1 is that

$$\int\limits_{A(z)}\int \left(\frac{1}{\mathrm{St}}\Theta_{0,t} - \Theta_{0,zz}\right) \mathrm{d}A = \int\limits_{s(z)} \left(-F(\Theta_0) + \frac{R_z\Theta_{0,z}}{\left(1 + \frac{R_\phi^2}{R^2}\right)^{1/2}}\right) \mathrm{d}s$$

or

$$\left(\frac{1}{\mathrm{St}}\Theta_{0,t} - \Theta_{0,zz}\right)\frac{\bar{R}^2 I_{2,0}}{2} = \bar{R}\bar{R}' I_{2,0}\Theta_{0,z} - \bar{R} I_{0,1} F(\Theta_0) \tag{15}$$

using (5). Combining (15) and the earlier results gives the zeroth-order problem[3]

$$\frac{1}{\mathrm{St}}\Theta_{0,t} - \Theta_{0,zz} = \frac{2}{\bar{R}}\left(\bar{R}'\Theta_{0,z} - \frac{I_{0,1}}{I_{2,0}}F(\Theta_0)\right), \quad 0 < z < S_0(t), \tag{16a}$$

$$\Theta_{0,z}(0, t) = \delta(\Theta_0(0, t) - \Theta_{\mathrm{ch}}), \tag{16b}$$

$$\Theta_0(S_0(t), t) = 1, \tag{16c}$$

$$S_0'(t) = \Theta_{0,z}(S_0(t), t) - \gamma, \quad S_0(0) = Z_0. \tag{16d}$$

4.2 Solution of the first-order model

With respect to the Neumann problem (14a)–(14b), in general, numerical methods need to be used to solve for Θ_1. However, in the case of weak anisotropy, i.e., $\alpha \ll 1$ in (5a), an approximate first-order model can be derived for $x \in \Omega(t)$, i.e, within the crystal. Denote

$$\Theta_1^*(r, \phi, z, t) = \Theta_1(r, \phi, z, t) - \frac{r^2}{2\bar{R}}\left(\bar{R}'\Theta_{0,z} - \frac{I_{0,1}}{I_{2,0}}F(\Theta_0)\right),$$

so that expressions (14a) and (16a) imply that

$$\Delta_{r\phi}\Theta_1^* = 0, \quad \mathbf{x} \in \Omega(t), \tag{17a}$$

and the boundary condition (14b) gives

$$\frac{\partial \Theta_1^*}{\partial \mathbf{n}_{r\phi}} = \left[\left(1 + \frac{R_\phi^2}{R^2}\right)^{-1/2}\frac{R}{\bar{R}}\frac{I_{0,1}}{I_{2,0}} - 1\right]F(\Theta_0) = \alpha\lambda F(\Theta_0) + O(\alpha^2), \tag{17b}$$

where we have used (5a) and noted that the coefficient of $\Theta_{0,z}$ vanishes identically. Motivated by the formal solution of (17a), we represent Θ_1^* as

$$\Theta_1^*(r, \phi, z, t) = \Theta_1^a(z, t) + \alpha\sum_{k=1}^{\infty} r^k\theta_k(z, t)\cos(k\phi + d_k) + O(\alpha^2), \tag{18}$$

[3] Expression (16a) is valid for all α. For weak anisotropy, $I_{0,1}/I_{2,0} = 1 + O(\alpha^2)$.

where $\Theta_1^a(z,t) = \Theta_1(r=0,z,t)$. Computing the direction derivative of (18) at the boundary $r = R(\phi, z)$ yields

$$\frac{\partial \Theta_1^*}{\partial \mathbf{n}_{r\phi}} = \alpha \left(1 + \frac{R_\phi^2}{R^2}\right)^{-\frac{1}{2}} \sum_{k=1}^{\infty} k R^{k-1} \theta_k \left(\cos(k\phi + d_k) + \frac{R_\phi}{R} \sin(k\phi + d_k)\right)$$
$$= \alpha \sum_{k=1}^{\infty} k \bar{R}^{k-1} \theta_k \cos(k\phi + d_k) + O(\alpha^2). \tag{19}$$

Comparing (17b) with (19) implies that θ_k is nontrivial only when $k \in \{n_j\}_{j=1}^m$ and in these cases, $d_k = \delta_k$, and $k\bar{R}^{k-1}\theta_k = \beta_k F(\Theta_0)$. Finally,

$$\Theta_1(r,\phi,z,t) = \Theta_1^a(z,t) + r^2 \Theta_1^b(z,t) + \alpha \Theta_1^c(r,\phi,z,t) + O(\alpha^2), \tag{20a}$$

where, keeping only those terms to $O(\alpha)$,

$$\Theta_1^b(z,t) = \frac{1}{2\bar{R}} \left(\bar{R}' \Theta_{0,z} - F(\Theta_0)\right), \tag{20b}$$

$$\Theta_1^c(r,\phi,z,t) = \bar{R} F(\Theta_0) \sum_{k=1}^{m} \frac{\beta_k}{n_k} \left(\frac{r}{\bar{R}}\right)^{n_k} \cos(n_k \phi + \delta_k). \tag{20c}$$

These last two terms are completely determined by Θ_0 and $\bar{R}$.

The derivation of the equations for $\Theta_1^a(z,t)$ proceeds in a similar fashion as in the zeroth-order model. In this case one uses (9) with $j = 1$ and (10b) so that

$$\Delta_{r\phi} \Theta_2 = \frac{1}{\mathrm{St}} \Theta_{1,t} - \Theta_{1,zz}, \quad \mathbf{x} \in \Omega(t), \tag{21a}$$

$$\frac{\partial \Theta_2}{\partial \mathbf{n}_{r\phi}} = -F'(\Theta_0)\Theta_1 + \frac{R_z \Theta_{1,z}}{\left(1 + \frac{R_\phi^2}{R^2}\right)^{1/2}} - \frac{1}{2} \frac{R_z^2 F(\Theta_0)}{\left(1 + \frac{R_\phi^2}{R^2}\right)}, \quad r = R(\phi, z). \tag{21b}$$

The compatibility condition and expression (20a) yield to $O(\alpha)$

$$\frac{1}{\mathrm{St}} \Theta_{1,t}^a = \Theta_{1,zz}^a + \frac{2}{\bar{R}} \left(\bar{R}' \Theta_{1,z}^a - F(\Theta_0)\right) + 2\bar{R} \left(\bar{R}' \Theta_{1,z}^b - F(\Theta_0)\right) - 2\bar{R}^2 \left[\frac{\bar{R}'^2}{\bar{R}} F(\Theta_0) + \left(\frac{1}{\mathrm{St}} \Theta_{1,t}^b - \Theta_{1,zz}^b\right)\right],$$
$$0 < z < S_0(t), \tag{22a}$$

where we note that Θ_1^c in (20a) is removed by the angular integration. The boundary and initial conditions ((11b) and (12b) evaluated at $r = 0$) read

$$\Theta_{1,z}^a(0,t) = \delta \Theta_1^a(0,t), \tag{22b}$$

$$\Theta_1^a(S_0(t),t) = -S_1(r=0,t)\Theta_{0,z}(S_0(t),t). \tag{22c}$$

The time evolution of $S_1(r,\phi,t)$ is governed by (13b) repeated here for convenience,

$$S_{1,t}(r,\phi,t) = \left(\Theta_{1,z} + S_1 \Theta_{0,zz} + \frac{\Theta_{1,r}^2}{\Theta_{0,z}} + \frac{\Theta_{1,\phi}^2}{r^2 \Theta_{0,z}}\right)\Bigg|_{z=S_0(t)}, \tag{22d}$$

with $S_1(r,\phi,0) = 0$ and Θ_1 given by (20).

Once again, the equations and boundary conditions of the temperature solutions are valid within the crystal $\Omega(t)$ at time t. To solve for them, we also need to find the boundary of the domain $\Omega(t)$, which consists of the solidification front S and the lateral surface R, as part of the solution procedure. When the Stefan number is relatively large, we can use the quasi-steady equations as approximations, which further simplifies the solution procedure. In this case, we can find the temperature solution at time t by solving a boundary-value problem with a moving boundary, instead of an initial-boundary-value problem.

Once the temperature field is obtained, we can proceed to estimate the thermal stress within the crystal $\Omega(t)$ at any given time t. In the next section, we will derive analytical formulas for the stress induced by the lateral temperature variation. These formulas are valid for any point $\mathbf{x}$ at any time t within the crystal $\Omega(t)$.

5 Thermal stress for isotropic solids

The thermal stress experienced by the crystal during its growth leads to the generation of structural defects in the crystal. In this paper, we focus on the stress due to lateral temperature variations. To simplify the discussion, we use the plane-strain assumption[4] in this paper and in the following discussion the displacement vector is denoted by $\mathbf{u} = (u^r, u^\phi)^{\mathrm{T}}$ in polar co-ordinates generalizing the discussion in [6].

5.1 Basic equations

Consider a two-dimensional (plane strain) thermoelastic problem with displacement $\mathbf{u}$ in polar coordinates. In this paper we will use the tensor and vector notations simultaneously, whenever it is convenient. By writing the stress tensor σ as

$$\sigma_{ij}^{\mathrm{tot}} = \sigma_{ij} - \frac{E\alpha_0}{1-2\nu}(T - T_g)\delta_{ij}, \tag{23}$$

where ν, E, and α_0 are respectively, the Poisson ratio, Young's modulus, and coefficient of thermal expansion, σ_{ij} satisfies

$$\sigma_{ij} = \frac{E}{1+\nu}\left(e_{ij} + \frac{\nu}{1-2\nu}e_{kk}\delta_{ij}\right), \quad e_{kk} = e_{rr} + e_{\phi\phi}, \tag{24}$$

where the non-trivial strains satisfy

$$e_{rr} = \frac{\partial u^r}{\partial r}, \quad e_{r\phi} = \frac{1}{2}\left(\frac{\partial u^\phi}{\partial r} - \frac{u^\phi}{r} + \frac{1}{r}\frac{\partial u^r}{\partial \phi}\right), \quad e_{\phi\phi} = \frac{1}{r}\frac{\partial u^\phi}{\partial \phi} + \frac{u^r}{r}, \tag{25}$$

and the equations of thermoelastic equilibrium, $\nabla \cdot \sigma^{\mathrm{tot}} := \sigma_{ij,j}^{\mathrm{tot}} = 0$, take the form

$$\frac{\partial \sigma_{rr}}{\partial r} + \frac{1}{r}\frac{\partial \sigma_{r\phi}}{\partial \phi} + \frac{\sigma_{rr} - \sigma_{\phi\phi}}{r} = \frac{\alpha_0 E}{1-2\nu}\frac{\partial (T - T_g)}{\partial r}, \tag{26a}$$

$$\frac{\partial \sigma_{r\phi}}{\partial r} + \frac{1}{r}\frac{\partial \sigma_{\phi\phi}}{\partial \phi} + \frac{2\sigma_{r\phi}}{r} = \frac{\alpha_0 E}{1-2\nu}\frac{1}{r}\frac{\partial (T - T_g)}{\partial \phi}, \tag{26b}$$

where $r < R(\phi, z)$ for $0 < z < S(t)$. By the scaling in Sect. 3.2 for r and T in addition to

$$(u^r, u^\phi) = \tilde{R}\alpha_0 \Delta T(\hat{u}^{\hat{r}}, \hat{u}^{\hat{\phi}}), \quad \sigma_{ij} = \frac{\alpha_0 \Delta T E}{1-\nu}\hat{\sigma}_{\hat{i}\hat{j}}, \quad e_{ij} = \alpha_0 \Delta T \hat{e}_{\hat{i}\hat{j}}, \quad \phi = \hat{\phi},$$

Eqs. 23 and 24 become, after dropping the hats for brevity,

$$\sigma_{ij}^{\mathrm{tot}} = \sigma_{ij} - \frac{1-\nu}{1-2\nu}\Theta\delta_{ij}, \tag{27}$$

$$\sigma_{ij} = \frac{1-\nu}{1+\nu}\left(e_{ij} + \frac{\nu}{1-2\nu}e_{kk}\delta_{ij}\right). \tag{28}$$

The equations of thermoelastic equilibrium (26) become

[4] Strictly speaking, the plane-strain assumption is valid for an infinitely long rod with temperature varying in the radial direction. For a crystal with a finite length and varying cross-sectional area, such as the one considered in this paper, plane strain is used as an approximation. Clearly, the assumption breaks down at the solid–liquid interface where the displacement does not vanish. However, as demonstrated in [36,Chap. 6] for the axisymmetric crystals, the plane-strain assumption leads to a reasonable approximation, provided that the aspect ratio and the axial variation of the cross-sectional area remain small. Near the solid–liquid interface, the results based on the plane-strain assumption are less accurate but the differences between the full numerical and the plane-strain solutions seem to stay bounded. Since the main objective of this paper is to investigate the effect of facets relative to the axisymmetric crystals, the plane-strain assumption will still provide useful insights despite its limitation.

$$\nabla \cdot \sigma = \mathbf{F} := \epsilon \frac{1-\nu}{1-2\nu} \nabla \Theta_1, \tag{29a}$$

or in component form

$$\frac{\partial \sigma_{rr}}{\partial r} + \frac{1}{r}\frac{\partial \sigma_{r\phi}}{\partial \phi} + \frac{\sigma_{rr} - \sigma_{\phi\phi}}{r} = \epsilon \frac{1-\nu}{1-2\nu}\frac{\partial \Theta_1}{\partial r}, \tag{29b}$$

$$\frac{\partial \sigma_{r\phi}}{\partial r} + \frac{1}{r}\frac{\partial \sigma_{\phi\phi}}{\partial \phi} + \frac{2\sigma_{r\phi}}{r} = \epsilon \frac{1-\nu}{1-2\nu}\frac{1}{r}\frac{\partial \Theta_1}{\partial \phi}. \tag{29c}$$

In the above expressions Θ has been replaced by $\epsilon\Theta_1$ which is the first nontrivial thermal contribution to the stress. Under the same scaling the stress-free boundary condition on the surface $r = R(\phi, z)$ with normal $\mathbf{n}$ becomes

$$\sigma \cdot \mathbf{n} = \mathbf{g} := \epsilon \frac{1-\nu}{1-2\nu} \Theta_1 \mathbf{n} \tag{30a}$$

which are (in component form)

$$\sigma_{rr} - \frac{R_\phi}{R}\sigma_{r\phi} = \epsilon \frac{1-\nu}{1-2\nu}\Theta_1, \quad r = R(\phi, z), \tag{30b}$$

$$\sigma_{r\phi} - \frac{R_\phi}{R}\sigma_{\phi\phi} = -\epsilon \frac{R_\phi}{R}\frac{1-\nu}{1-2\nu}\Theta_1, \quad r = R(\phi, z), \tag{30c}$$

where

$$\Theta_1(r, \phi, z, t) = \Theta_1^a(z, t) + r^2\Theta_1^b(z, t) + \alpha\Theta_1^c(r, \phi, z, t) + O(\alpha^2).$$

A useful shorthand notation, especially in the anisotropic case, is to represent the non-dimensional versions of the strain-displacement (25) and stress–strain (28) relationships as

$$\mathbf{e} = \mathbf{S}(\mathbf{u}), \quad \boldsymbol{\sigma} = C_0\mathbf{S}(\mathbf{u}), \tag{31}$$

respectively, with the subscript zero on the stiffness matrix, C_0, indicating isotropy. By further defining the operators

$$\mathcal{L}_0 := \nabla \cdot C_0\mathbf{S}, \quad \mathcal{B}_0 := C_0\mathbf{S} \cdot \mathbf{n}, \tag{32}$$

we can restate the equilibrium equations (29) and boundary conditions (30) as the boundary-value problem

$$\mathcal{L}_0(\mathbf{u}) = \mathbf{F}, \quad \mathbf{x} \in \Omega(t), \tag{33a}$$

$$\mathcal{B}_0(\mathbf{u}) = \mathbf{g}, \quad r = R(\phi, z). \tag{33b}$$

In practice, a complete set of solutions to (29) can be constructed with the functions Φ, and $\boldsymbol{\Psi} = (\psi_1, \psi_2)$ [37, pp. 83–84], [38]. These are based on the observation that provided ψ_1, ψ_2 are harmonic and

$$\nabla\left(\Delta_{r\phi}\Phi\right) = \frac{(1+\nu)(1-2\nu)}{(1-\nu)^2}\mathbf{F}, \tag{34}$$

then a solution to (33) is given by the displacement vector

$$\mathbf{u} = \nabla\left(\Phi + \mathbf{r} \cdot \boldsymbol{\Psi}\right) - 4(1-\nu)\boldsymbol{\Psi}, \tag{35}$$

where $\mathbf{r}$ is a position vector. The components of the stress tensor are found using (31).

5.2 Perturbation solution of the thermoelastic equations

Based on the assumption of $\alpha \ll 1$, we assume that the displacement has the following approximation:

$$u^r \sim u_0^r + \alpha u_1^r + \alpha^2 u_2^r + \cdots, \quad u^\phi \sim u_0^\phi + \alpha u_1^\phi + \alpha^2 u_2^\phi + \cdots. \tag{36}$$

Applying (36) to (29) and expanding in powers of α gives a sequence of approximations to the thermoelastic problem. In the following, $\sigma_{ij}^n = \sigma_{ij}^n(u_n^r, u_n^\phi)$ denotes the components of the stress tensor generated by the displacement (u_n^r, u_n^ϕ). We find that σ_{ij}^0 (analytically extended to $r < \bar{R}(z)$) satisfy

$$\frac{\partial \sigma_{rr}^0}{\partial r} + \frac{1}{r}\frac{\partial \sigma_{r\phi}^0}{\partial \phi} + \frac{\sigma_{rr}^0 - \sigma_{\phi\phi}^0}{r} = 2\epsilon \frac{1-\nu}{1-2\nu} r\Theta_1^b, \quad r < \bar{R}(z), \tag{37a}$$

$$\frac{\partial \sigma_{r\phi}^0}{\partial r} + \frac{1}{r}\frac{\partial \sigma_{\phi\phi}^0}{\partial \phi} + \frac{2\sigma_{r\phi}^0}{r} = 0, \quad r < \bar{R}(z), \tag{37b}$$

with the boundary conditions

$$\sigma_{rr}^0 = \epsilon \frac{1-\nu}{1-2\nu} \bar{R}^2 \Theta_1^b, \quad r = \bar{R}(z), \tag{38a}$$

$$\sigma_{r\phi}^0 = 0, \quad r = \bar{R}(z). \tag{38b}$$

Solving for σ_{ij}^0 we choose $\epsilon\Theta_1 = \epsilon r^2 \Theta_1^b = f(r)$ in (34) so that

$$\Delta_{r\phi}\Phi = \frac{1+\nu}{1-\nu}\left(f(r) + A_0\right)$$

with A_0 some constant to be determined. Setting $\psi_1 = \psi_2 = 0$, we have that Eqs. 35 and 38 give the displacement components

$$\mathbf{u}_0 = \frac{1+\nu}{1-\nu}\frac{\epsilon r \Theta_1^b}{4}\begin{pmatrix} \bar{R}^2(1-2\nu) + r^2 \\ 0 \end{pmatrix} \tag{39}$$

as in [6]. Using (31) yields

$$\begin{pmatrix} \sigma_{rr}^0 \\ \sigma_{\phi\phi}^0 \\ \sigma_{r\phi}^0 \end{pmatrix} = \frac{1}{4}\epsilon\Theta_1^b \begin{pmatrix} \bar{R}^2 - r^2 \\ \bar{R}^2 - 3r^2 \\ 0 \end{pmatrix} + \epsilon \frac{1-\nu}{1-2\nu} r^2 \Theta_1^b \begin{pmatrix} 1 \\ 1 \\ 0 \end{pmatrix}. \tag{40}$$

In a similar fashion, σ_{ij}^1 satisfy

$$\frac{\partial \sigma_{rr}^1}{\partial r} + \frac{1}{r}\frac{\partial \sigma_{r\phi}^1}{\partial \phi} + \frac{\sigma_{rr}^1 - \sigma_{\phi\phi}^1}{r} = \epsilon \frac{1-\nu}{1-2\nu}\frac{\partial \Theta_1^c}{\partial r}, \quad r < \bar{R}(z), \tag{41a}$$

$$\frac{\partial \sigma_{r\phi}^1}{\partial r} + \frac{1}{r}\frac{\partial \sigma_{\phi\phi}^1}{\partial \phi} + \frac{2\sigma_{r\phi}^1}{r} = \epsilon \frac{1-\nu}{1-2\nu}\frac{1}{r}\frac{\partial \Theta_1^c}{\partial \phi}, \quad r < \bar{R}(z), \tag{41b}$$

with the boundary conditions

$$\sigma_{rr}^1 - \lambda'\sigma_{r\phi}^0 + \lambda\bar{R}\frac{\partial \sigma_{rr}^0}{\partial r} = \epsilon\frac{1-\nu}{1-2\nu}\Theta_1^c + 2\lambda\epsilon\frac{1-\nu}{1-2\nu}\bar{R}^2\Theta_1^b, \quad r = \bar{R}(z), \tag{42a}$$

$$\sigma_{r\phi}^1 - \lambda'\sigma_{\phi\phi}^0 + \lambda\bar{R}\frac{\partial \sigma_{r\phi}^0}{\partial r} = -\lambda'\epsilon\frac{1-\nu}{1-2\nu}\bar{R}^2\Theta_1^b, \quad r = \bar{R}(z). \tag{42b}$$

To solve for σ_{ij}^1 we first consider, without loss of generality, the kth component of Θ_1^c. At this point it is convenient to introduce the notation $(\mathcal{C}_k, \mathcal{S}_k) = (\cos(n_k\phi + \delta_k), \sin(n_k\phi + \delta_k))$ and the generalization $(\tilde{\mathcal{C}}_k, \tilde{\mathcal{S}}_k)$ with $\tilde{n}_k$ replacing n_k. In this notation (5) and (20) give

$$\lambda = \sum_{k=1}^m \beta_k \mathcal{C}_k, \quad \lambda' = -\sum_{k=1}^m \beta_k n_k \mathcal{S}_k, \quad \Theta_1^c = \bar{R}F(\Theta_0)\sum_{k=1}^m \frac{\beta_k}{n_k}\left(\frac{r}{\bar{R}}\right)^{n_k}\mathcal{C}_k. \tag{43}$$

Furthermore, using (40) to simplify (42),

$$\sigma_{rr}^1 = 2C_1\beta_k\mathcal{C}_k + 4\frac{1-\nu}{1-2\nu}\frac{C_2\beta_k}{n_k}\mathcal{C}_k, \quad r = \bar{R}(z), \tag{44a}$$

$$\sigma_{r\phi}^1 = 2C_1\beta_k n_k \mathcal{S}_k, \quad r = \bar{R}(z), \tag{44b}$$

where

$$C_1 = \frac{1}{4}\epsilon \bar{R}^2 \Theta_1^b, \quad C_2 = \frac{1}{4}\epsilon \bar{R} F(\Theta_0). \tag{45}$$

We let $\sigma_{ij}^1 = \sigma_{ij}^{1,p} + \sigma_{ij}^{1,h}$ where $\sigma_{ij}^{1,p}$ is a particular solution of (41), and $\sigma_{ij}^{1,h}$ is a homogeneous solution of (41) with a boundary condition that combines the particular solution and (44).

For $\sigma_{ij}^{1,p}$, setting $\psi_1 = \psi_2 = 0$, and choosing an appropriate Φ, one obtains from (35) the displacement

$$\mathbf{u}_{1,p} = \frac{1+\nu}{1-\nu}\frac{C_2\beta_k\bar{R}}{n_k(n_k+1)}\left(\frac{r}{\bar{R}}\right)^{n_k+1}\begin{pmatrix}(n_k+2)\mathcal{C}_k\\ -n_k\mathcal{S}_k\end{pmatrix}. \tag{46}$$

Using (31),

$$\begin{pmatrix}\sigma_{rr}^{1,p}\\ \sigma_{\phi\phi}^{1,p}\\ \sigma_{r\phi}^{1,p}\end{pmatrix} = C_2\beta_k\left(\frac{r}{\bar{R}}\right)^{n_k}\begin{pmatrix}\left(1+\dfrac{2}{n_k(1-2\nu)}\right)\mathcal{C}_k\\ \left(-1+\dfrac{2}{n_k(1-2\nu)}\right)\mathcal{C}_k\\ -\mathcal{S}_k\end{pmatrix}. \tag{47}$$

This leaves $\sigma_{ij}^{1,h}$ which satisfies the homogeneous plate elasticity equation with boundary conditions

$$\sigma_{rr}^{1,h} = \left(2C_1 - \frac{(n_k-2)}{n_k}C_2\right)\beta_k\mathcal{C}_k, \quad r = \bar{R}(z), \tag{48a}$$

$$\sigma_{r\phi}^{1,h} = (2n_kC_1 + C_2)\beta_k\mathcal{S}_k, \quad r = \bar{R}(z). \tag{48b}$$

To match the boundary condition using (35), we combine ψ_1 and ψ_2 into a single harmonic function Φ_1. To this end we choose ψ_1 and ψ_2 so that $\nabla\cdot(\psi_1, -\psi_2) = 0$. Assigning $\nabla\Phi_1 = (\psi_1, -\psi_2)$, implies $\Delta\Phi_1 = 0$ provided $\psi_1 = \Phi_{1,x}$, $\psi_2 = -\Phi_{1,y}$. Writing (35) in polar coordinates, we find

$$\mathbf{u}_{1,h} = \begin{pmatrix}\dfrac{\partial\Phi}{\partial r}\\ \dfrac{1}{r}\dfrac{\partial\Phi}{\partial\phi}\end{pmatrix} + (3-4\nu)\begin{pmatrix}-\dfrac{\partial\Phi_1}{\partial r}\cos 2\phi + \dfrac{\partial\Phi_1}{\partial\phi}\dfrac{\sin 2\phi}{r}\\ \dfrac{\partial\Phi_1}{\partial r}\sin 2\phi + \dfrac{\partial\Phi_1}{\partial\phi}\dfrac{\cos 2\phi}{r}\end{pmatrix} + r\mathbf{G}, \tag{49}$$

where

$$\mathbf{G} = \begin{pmatrix}\dfrac{\partial^2\Phi_1}{\partial r^2}\cos^2\phi + \left(\dfrac{\partial\Phi_1}{\partial r} + \dfrac{1}{r}\dfrac{\partial^2\Phi_1}{\partial\phi^2}\right)\dfrac{\sin^2\phi}{r} - \left(\dfrac{\partial^2\Phi_1}{\partial r\partial\phi} - \dfrac{1}{r}\dfrac{\partial\Phi_1}{\partial\phi}\right)\dfrac{\sin 2\phi}{r}\\ \left(\dfrac{\partial^2\Phi_1}{\partial r^2} - \dfrac{1}{r}\dfrac{\partial\Phi_1}{\partial r} - \dfrac{1}{r^2}\dfrac{\partial^2\Phi_1}{\partial\phi^2}\right)\cos\phi\sin\phi + \left(\dfrac{\partial^2\Phi_1}{\partial r\partial\phi} - \dfrac{1}{r}\dfrac{\partial\Phi_1}{\partial\phi}\right)\dfrac{\cos 2\phi}{r}\end{pmatrix}.$$

By representing Φ and Φ_1 as

$$\Phi_1(r,\phi) = \sum_{k=1}^{\infty} P_k r^k\cos(k\phi + a_k), \quad \Phi(r,\phi) = \sum_{k=1}^{\infty} Q_k r^k\cos(k\phi + b_k), \tag{50}$$

where P_k, Q_k, a_k, and b_k are arbitrary constants independent of r and ϕ, expression (49) implies that

$$\mathbf{u}_{1,h} = \sum_{k=1}^{\infty} kr^{k-1}\begin{pmatrix}(k-4+4\nu)P_k\cos((k-2)\phi + a_k) + Q_k\cos(k\phi + b_k)\\ (4\nu - k - 2)P_k\sin((k-2)\phi + a_k) - Q_k\sin(k\phi + b_k)\end{pmatrix}. \tag{51}$$

Applying (31) once again yields

$$\begin{pmatrix}\sigma_{rr}^{1,h}\\ \sigma_{\phi\phi}^{h}\\ \sigma_{r\phi}^{1,h}\end{pmatrix} = \frac{1-\nu}{1+\nu}\sum_{k=1}^{\infty} k(k-1)r^{k-2}\begin{pmatrix}(k-4)P_k\cos((k-2)\phi + a_k) + Q_k\cos(k\phi + b_k)\\ -kP_k\cos((k-2)\phi + a_k) - Q_k\cos(k\phi + b_k)\\ (2-k)P_k\sin((k-2)\phi + a_k) - Q_k\sin(k\phi + b_k)\end{pmatrix}. \tag{52}$$

Imposing the boundary condition (48) we conclude that the only non-zero terms are associated with P_{n_k+2}, Q_{n_k}, a_{n_k+2}, b_{n_k} and $a_{n_k+2} = b_{n_k} = \delta_k$. Furthermore, P_{n_k+2}, Q_{n_k} satisfy:

$$\begin{pmatrix} (n_k+2)(n_k+1)(n_k-2)n_k(n_k-1) \\ -(n_k+2)(n_k+1)n_k - n_k(n_k-1) \end{pmatrix} \begin{pmatrix} \bar{R}_k^n P_{n_k+2} \\ \bar{R}^{n_k-2} Q_{n_k} \end{pmatrix} = \frac{1+\nu}{1-\nu}\beta_k \begin{pmatrix} 2C_1 - \frac{n_k-2}{n_k}C_2 \\ 2n_k C_1 + C_2 \end{pmatrix}$$

and on solving for P_{n_k+2}, Q_{n_k} we find

$$\begin{pmatrix} \sigma_{rr}^{1,h} \\ \sigma_{\phi\phi}^{1,h} \\ \sigma_{r\phi}^{1,h} \end{pmatrix} = \beta_k \begin{pmatrix} \left(\frac{n_k(n_k-1)C_1 r^{n_k-2}}{\bar{R}^{n_k-2}} + \frac{(n_k(n_k+1)C_1 + C_2)\,(2-n_k) r^{n_k}}{n_k \bar{R}^{n_k}} \right) \mathcal{C}_k \\ \left(\frac{n_k(1-n_k)C_1 r^{n_k-2}}{\bar{R}^{n_k-2}} + \frac{(n_k(n_k+1)C_1 + C_2)\,(n_k+2) r^{n_k}}{n_k \bar{R}^{n_k}} \right) \mathcal{C}_k \\ \left(\frac{n_k(1-n_k)C_1 r^{n_k-2}}{\bar{R}^{n_k-2}} + \frac{(n_k(n_k+1)C_1 + C_2)\, r^{n_k}}{\bar{R}^{n_k}} \right) \mathcal{S}_k \end{pmatrix}. \tag{53}$$

The displacement is obtained by combining (39), (46) and (51) with restrictions on P_k, Q_k to yield

$$\mathbf{u}_0 + \alpha \mathbf{u}_1 = \begin{pmatrix} r D_r^{(1)} + r^3 D_r^{(3)} \\ 0 \end{pmatrix} + r^{n_k-1} \begin{pmatrix} D_r^- \mathcal{C}_k \\ D_\phi^- \mathcal{S}_k \end{pmatrix} + r^{n_k+1} \begin{pmatrix} D_r^+ \mathcal{C}_k \\ D_\phi^+ \mathcal{S}_k \end{pmatrix}, \tag{54}$$

where

$$D_r^{(1)} = \left(\frac{1+\nu}{1-\nu} \right) C_1(1-2\nu), \quad D_r^{(3)} = \left(\frac{1+\nu}{1-\nu} \right) \frac{C_1}{\bar{R}^2}, \tag{55a}$$

$$D_r^- = \left(\frac{1+\nu}{1-\nu} \right) \frac{C_1 \alpha \beta_k}{\bar{R}^{n_k-2}} n_k, \quad D_\phi^- = -\left(\frac{1+\nu}{1-\nu} \right) \frac{C_1 \alpha \beta_k}{\bar{R}^{n_k-2}} n_k, \tag{55b}$$

$$D_r^+ = \left(\frac{1+\nu}{1-\nu} \right) \frac{C_1 \alpha \beta_k}{\bar{R}^{n_k}} (2 - 4\nu - n_k) + \frac{4(1+\nu)}{n_k(n_k+1)} \frac{C_2 \alpha \beta_k}{\bar{R}^{n_k}}, \tag{55c}$$

$$D_\phi^+ = \left(\frac{1+\nu}{1-\nu} \right) \frac{C_1 \alpha \beta_k}{\bar{R}^{n_k}} (4 - 4\nu + n_k) + \frac{4(1+\nu)}{n_k(n_k+1)} \frac{C_2 \alpha \beta_k}{\bar{R}^{n_k}}. \tag{55d}$$

Combining (27), (40), (47), and (53) yields the components of the total stress

$$\begin{pmatrix} \sigma_{rr}^{\text{tot}} \\ \sigma_{\phi\phi}^{\text{tot}} \\ \sigma_{r\phi}^{\text{tot}} \end{pmatrix} = C_1 \begin{pmatrix} 1 - \left(\frac{r}{\bar{R}} \right)^2 \\ 1 - 3\left(\frac{r}{\bar{R}} \right)^2 \\ 0 \end{pmatrix} + \alpha C_1 \beta_k n_k (n_k - 1) \left(\frac{r}{\bar{R}} \right)^{n_k-2} \begin{pmatrix} \mathcal{C}_k \\ -\mathcal{C}_k \\ -\mathcal{S}_k \end{pmatrix} + \alpha C_1 \beta_k (n_k+1) \left(\frac{r}{\bar{R}} \right)^{n_k} \begin{pmatrix} (2-n_k)\mathcal{C}_k \\ (n_k+2)\mathcal{C}_k \\ n_k \mathcal{S}_k \end{pmatrix}. \tag{56a}$$

Since $e_{zz} = 0$, the stress–strain relation (28) with (27) implies that

$$\sigma_{zz}^{\text{tot}} = \nu(\sigma_{rr}^{\text{tot}} + \sigma_{\phi\phi}^{\text{tot}}) - (1-\nu)\epsilon\Theta_1.$$

Using (56a) gives

$$\sigma_{zz}^{\text{tot}} = 2C_1 \left(1 - 2\left(\frac{r}{\bar{R}} \right)^2 \right) + 4\alpha\beta_k \left(\nu(n_k+1)C_1 - \frac{1-\nu}{n_k} C_2 \right) \left(\frac{r}{\bar{R}} \right)^{n_k} \mathcal{C}_k, \tag{56b}$$

where we have also added the quantity $2C_1(1-\nu)$, using Saint Venant's principle, so that the average of σ_{zz}^{tot} over the surface $A(z)$ is zero.

5.3 The von Mises and total resolved stress

A characteristic amount of stress can be assigned to each point with the von Mises stress which satisfies

$$2\sigma_{\text{vm}}^2 = (\sigma_1 - \sigma_2)^2 + (\sigma_1 - \sigma_3)^2 + (\sigma_2 - \sigma_3)^2 = (\sigma_{rr} - \sigma_{\phi\phi})^2 + (\sigma_{rr} - \sigma_{zz})^2 + (\sigma_{\phi\phi} - \sigma_{zz})^2 + 6\sigma_{r\phi}^2 \tag{57}$$

where $\sigma_1, \sigma_2, \sigma_3$ denote the eigenvalues of the stress tensor given by (56).

The preferred method of dislocation generation in all III–V semiconductors, is through the generation of slip defects, in particular the $\{111\}$, $\langle 1\bar{1}0\rangle$ slip system [6]. Consisting of four glide planes within which atoms can slip in one of three directions, the resolved stress $\sigma_{\rm rs}$, in a particular slip direction $\vec{g}$ within the glide plane with normal $\vec{n}$ is given by

$$\sigma_{\rm rs} = \vec{g}^T U_{\mathbf{p}}^T Q^T \sigma^{\rm tot} Q U_{\mathbf{p}} \vec{n}.$$

The matrix $U_{\mathbf{p}}$ rotates vectors from the crystallographic frame to the solidification frame so that for a given pulling direction, the rows of $U_{\mathbf{p}}$ are the vectors $\mathbf{a}$, $\mathbf{b}$ and $\mathbf{p}$. If the stress tensor $\sigma^{\rm tot}$ is expressed in the (r, ϕ, z) coordinates, Q is the coordinate transformation matrix that takes $(x, y, z) \to (r, \phi, z)$.

Plastic deformation of the crystal occurs if the stress in any of the 12 slip directions exceeds a maximum value known as the critical resolved shear stress, $\sigma_{\rm crss}$. To leading order, the actual density of dislocations suffered by the crystal is proportional to the total excess stress at any given point within the crystal. In this sense, an estimation of where dislocations are likely to occur is given by the distribution of the total absolute resolved stress

$$|\sigma_{\rm rs}^{\rm tot}| = \sum_{i=1}^{12} \left| \vec{g}_i^T U_{\mathbf{p}}^T Q^T \sigma^{\rm tot} Q U_{\mathbf{p}} \vec{n}_i \right|. \tag{58}$$

6 Numerical results

The base geometry for the computation is a cone so that $\bar{R}(z) = \bar{R}(Z_0) + \mu_{\rm cone} z$. Starting with a seed with length and radius of 0.005 m and choosing a 1/2 opening angle of $\varphi_{\rm cone} = 5^\circ$ gives a final radius of 0.0286 m for a crystal of final length 0.3 m. Converting to non-dimensional coordinates ($\tilde{R} = 0.03$ m, $\epsilon = 0.026$) gives a non-dimensional $\mu_{\rm cone} = 0.496$.

For the thermal model, Θ_0 is the solution of (16) in the pseudo-steady case ($1/{\rm St} = 0$) with $\delta = \gamma = 0$ and $I_{0,1}/I_{2,0} = 1$. Θ_1 is given by (20) with $h_F = 0$, $h_{\rm gs} = \bar{h}_{\rm gs} = 1$ so that $F(\Theta) = \beta\Theta = \Theta$. Also, Θ_1^c is defined by the data in Table 1, Θ_1^b is derived from Θ_0 and Θ_1^a satisfies (22). The Biot number is taken as $\epsilon = 0.026$.

We present the distribution of $\sigma_{\rm rs}^{\rm tot}$ as given by (58) with the total stress given by (56). The values of E and ν are chosen to be those associated with the $\{111\}$ planes since these are invariant quantities for crystals with cubic symmetry [39] as well as being responsible for generating the slip defects within these crystals. These values are given by

$$E_{\{111\}} = \frac{4(C_{11}+2C_{12})(C_{11}-C_{12})C_{44}}{(C_{11}+2C_{12})(C_{11}-C_{12})+2C_{11}C_{44}} = 6.20 \times 10^4 \text{ MPa}, \tag{59a}$$

$$\nu_{\{111\}} = \frac{1}{3}\frac{(C_{11}+2C_{12})(C_{11}-C_{12})-2C_{44}(C_{11}-4C_{12})}{(C_{11}+2C_{12})(C_{11}-C_{12})+2C_{11}C_{44}} = 0.362, \tag{59b}$$

where we have used the stiffness constants for InSb: $C_{11} = 6.70 \times 10^4$, $C_{12} = 3.65 \times 10^4$, $C_{44} = 3.02 \times 10^4$ MPa. When combined with the parameters above, the dimensional constant for the stress calculations is $\alpha_0 \Delta T E/(1-\nu) \sim 106$ MPa.

In Fig. 5, we plot the contours of the resolved stress for crystals pulled at the [001] direction. Since the cross-section is circular, the solution obtained previously in [6] applies. In Figs. 6 and 7, we plotted the contours of the resolved stress for crystals grown by pulling the seeds in the $[\bar{1}\bar{1}\bar{1}]$ and $[\bar{2}11]$ directions, respectively. In both cases, stress is plotted for both circular and faceted cross-sections. As it can be seen from the plots, facet formation has a visible effect on the thermal stress inside these crystals. The maximum values of the stress are bigger in crystals with facets. In addition, higher stress levels are more concentrated close to the lateral surface for these crystals. Our results suggest that the axisymmetric calculation [6] may under predict the thermal stress for certain seed orientations.

Among the three seeding orientations considered in this study, the effect of facet formation on the stress is much stronger for the $[\bar{1}\bar{1}\bar{1}]$ pulling direction than that for the $[\bar{2}11]$ pulling direction. The $[\bar{1}\bar{1}\bar{1}]$ direction not only

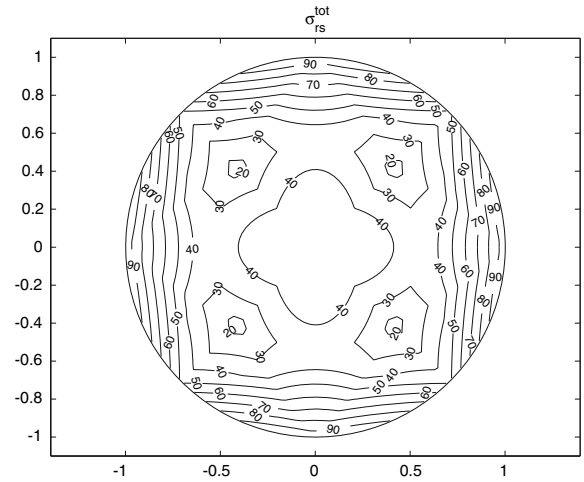

Fig. 5 Total resolved-stress distribution just inside the crystal–melt interface at the end of the growth for a crystal pulled in the [001] direction. All reported stress values are expressed in percent with 100% occurring at the outer edge of a crystal grown in the [001] direction. For this orientation $\max|\sigma_{\mathrm{rs}}^{\mathrm{tot}}| = 9.18 \times 10^{-3}$ and $\min|\sigma_{\mathrm{rs}}^{\mathrm{tot}}| = 1.48 \times 10^{-3}$ corresponding to 0.975 and 0.159 MPa, respectively

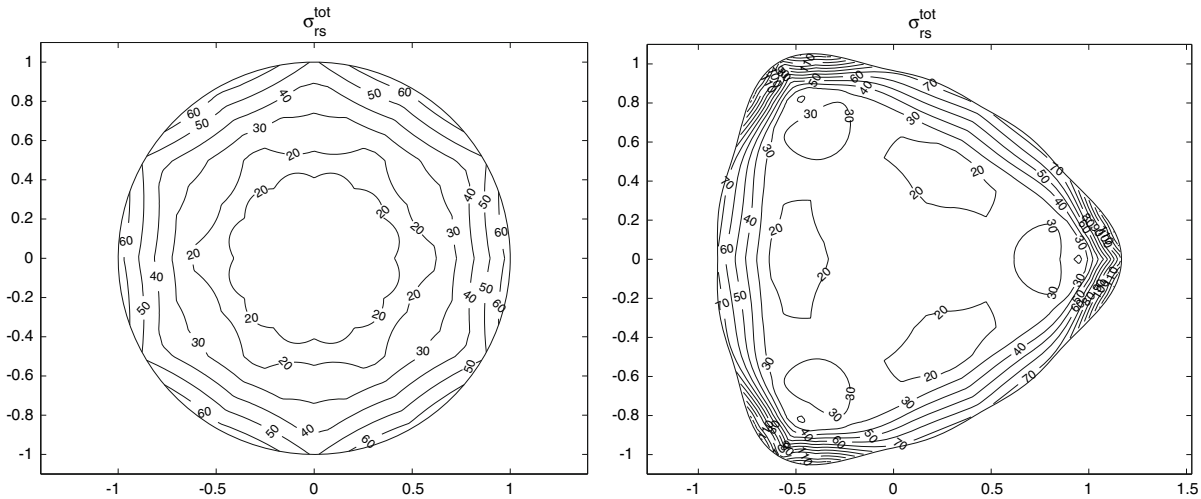

Fig. 6 Total resolved-stress distribution just inside the crystal–melt interface at the end of the growth for a crystal pulled in the $[\bar{1}\bar{1}\bar{1}]$ direction with and without facets. For this orientation $\max|\sigma_{\mathrm{rs}}^{\mathrm{tot}}| = 13.1 \times 10^{-3}$ and $\min|\sigma_{\mathrm{rs}}^{\mathrm{tot}}| = 1.19 \times 10^{-3}$ corresponding to 1.39 and 0.126 MPa, respectively

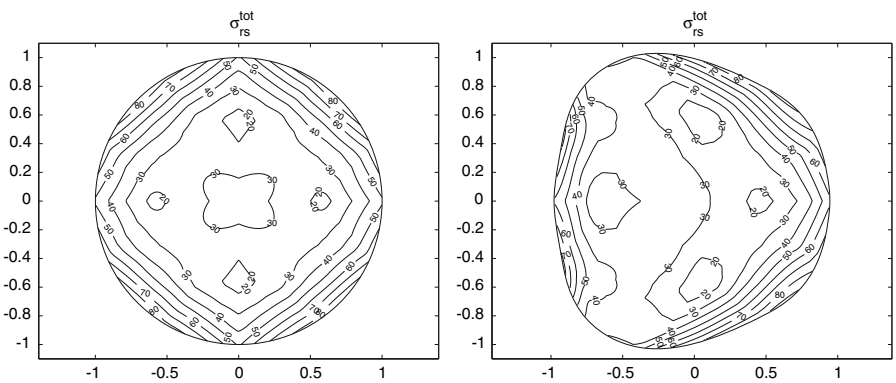

Fig. 7 Total resolved-stress distribution just inside the crystal–melt interface at the end of the growth for a crystal pulled in the $[\bar{2}11]$ direction with and without facets. For this orientation $\max|\sigma_{\mathrm{rs}}^{\mathrm{tot}}| = 8.63 \times 10^{-3}$ and $\min|\sigma_{\mathrm{rs}}^{\mathrm{tot}}| = 1.28 \times 10^{-3}$ corresponding to 0.916 and 0.135 MPa, respectively

produces higher stresses, but also a more extensive region of high stresses. Despite facet formation, the maximum stress for the $[\bar{2}11]$ orientation is in fact lower than that for the [001] orientation without facets. This observation indicates that the $[\bar{1}\bar{1}\bar{1}]$ orientation should be avoided while the $[\bar{2}11]$ direction should be favored.

7 Conclusion

In this paper we have proposed a novel model to predict facet formation for constrained crystal growth such as the Czochralski process. The model used a geometric argument based on the crystal-lattice structure and facets are predicted for crystals in the $[\bar{1}\bar{1}\bar{1}]$ and $[\bar{2}11]$ seeding directions but not in the [001] direction, for a given growth angle. Since the anisotropic effect due to facet formation is weak, a domain perturbation method is used to derive thermal stress, as a generalization of the approach used in a previous study for axisymmetric crystals [6]. Numerical results show that facet formation greatly affects thermal stress distribution and defects are more likely to form in faceted crystals with certain seed orientations due to high stress levels while other orientations may be favored because of reduced stress levels.

As we alluded to earlier, we have made a number of simplifying assumptions in this paper, e.g., plane strain for thermal stress. While the results we have obtained with these assumptions provide useful insights, it is desirable to re-examine the effects of these assumptions. As a next step, we plan to systematically derive the formula for thermal stress using boundary-layer analysis as well as the small-aspect-ratio asymptotic expansion. In this case, the plane-strain formula will be the leading-order solution and the higher-order solutions could be obtained as a correction to the plane-strain solution. In addition, from a practical point of view, a real-time solution would be more relevant, compared to the solution based on an equilibrium shape. This will be done by applying the current growth model to a dynamic growth process from an arbitrary initial cross-sectional shape, instead of an equilibrium one, with a time-dependent growth angle.

Finally, in the current model, corners form at the intersection of facets. We have applied an ad hoc smoothing technique to regularize the corners. In the future, we plan to incorporate physical mechanisms such as intrinsic curvature and elastic energy into our geometric approach.

Acknowledgment The authors would like to acknowledge the support from NSERC (HH and CSB), MITACS (HH and JW), and Firebird Inc. (HH and CSB). We would also like to thank the referees and handling editor of JEM for their constructive comments.

Appendix: Construction of the lateral-growth function f

f is the ratio of the lateral to axial growth rate as determined by the unit cell of InSb as shown in Fig. 2. The speed in a given direction $\hat{\mathbf{d}}$ is proportional to the thickness of the shell $\Delta r(\hat{\mathbf{d}})$ between two complete tetrahedrons formed of unit cells. It is convenient to denote these eight planes, four original, four after adding a layer, as $\hat{\mathbf{n}}_i \circ \mathbf{r} = s_i$ and $\hat{\mathbf{n}}_i \circ \mathbf{r} = t_i$, respectively, with $\mathbf{r} = \langle x, y, z\rangle$ where the parameters are summarized in the table.

i	$\hat{\mathbf{n}}_i$	s_i	t_i
1	$\frac{1}{\sqrt{3}}\langle 1, 1, 1\rangle$	$\frac{2a}{\sqrt{3}}$	$\frac{a}{\sqrt{3}}$
2	$\frac{1}{\sqrt{3}}\langle 1, 1, -1\rangle$	$\frac{a}{\sqrt{3}}$	$\frac{2a}{\sqrt{3}}$
3	$\frac{1}{\sqrt{3}}\langle 1, -1, 1\rangle$	$\frac{a}{\sqrt{3}}$	$\frac{2a}{\sqrt{3}}$
4	$\frac{1}{\sqrt{3}}\langle -1, 1, 1\rangle$	$\frac{a}{\sqrt{3}}$	$\frac{2a}{\sqrt{3}}$

In this case the centre of the original tetrahedron is $Q(3a/4, 3a/4, 3a/4)$ where the length of the unit cell is a. The thickness of the shell $\Delta r(\hat{\mathbf{d}})$ can be defined as

$$\frac{1}{\Delta r(\hat{\mathbf{d}})} = \max_{i\in\{1,2,3,4\}} \frac{\hat{\mathbf{n}}_i \circ \hat{\mathbf{d}}}{t_i - s_i}.$$

Once we have the thickness, the speed in a given direction is found using $v(\hat{\mathbf{d}})\Delta t = \Delta r(\hat{\mathbf{d}})$. Notice that the tetrahedron is orientated so that there is a vertex in the [111] outward direction and a face in the $[\bar{1}\bar{1}\bar{1}]$ direction. For a typical face, let $\hat{\mathbf{d}} = -\langle 1, 1, 1\rangle/\sqrt{3}$ and $i = 1$ to find that $v_{\text{face}} = \Delta r_{\text{face}}/\Delta t = (a/\Delta t)\sqrt{3}/3$. For a vertex, let $\hat{\mathbf{d}} = \langle 1, 1, 1\rangle/\sqrt{3}$ and $i \neq 1$ to give $v_{\text{vertex}} = \Delta r_{\text{vertex}}/\Delta t = (a/\Delta t)\sqrt{3}$. This shows that with no external constraints, the growth rate in the direction of the vertices is three times that of the faces. Since we are only interested in relative speeds, we take $a/\Delta t = \sqrt{3}$ so that $v_{\text{face}} \equiv 1$. For a direction $\hat{\mathbf{d}}$ in the plane of the melt surface with an outward normal given by $\hat{\mathbf{p}}$ (the pulling direction), one has $f(\hat{\mathbf{d}}) = \Delta r(\hat{\mathbf{d}})/\Delta r(-\hat{\mathbf{p}})$.

References

1. Chen T, Wu H, Weng C (1997) The effect of interface shape on anisotropic thermal stress of bulk single crystal during Czochralski growth. J Cryst Growth 173(3–4):367–379
2. Miyazaki N (2002) Development of a thermal stress analysis system for anisotropic single crystal growth. J Cryst Growth 236(1–3):455–465
3. Vigdergauz S, Givoli D (1999) Thermoelastic stresses in a crystal with weak anisotropy. J Cryst Growth 198–199(Part 1):125–128
4. Vigdergauz S, Givoli D (1999) Thermoelastic stresses in a cylinder or disk with cubic anisotropy. Int J Solids Struct 36(14):2109–2125
5. Micklethwaite WFH (2005) The bulk growth of InSb & related ternary alloys. In: Capper P (ed) Bulk crystal growth of electronic, optical and optoelectronic materials, chap 5. Wiley, New Jersey
6. Bohun CS, Frigaard IA, Huang H, Liang S (2006) A semianalytical thermal stress model for the Czochralski growth of type III–V compounds. SIAM J Appl Math 66(5):1533–1562
7. Russo G, Smereka P (2000) A level-set method for the evolution of faceted crystals. SIAM J Sci Comput 21(6):2073–2095
8. Pet'kov IS, Red'kin BS (1993) Calculation of the stationary cross-section form of nonaxisymmetrical crystals growing from the melt. J Cryst Growth 131(3–4):598–606
9. Davis SH (2001) Theory of solidification. Cambridge University Press, Cambridge
10. Golovin AA, Davis SH (1998) Effect of anisotropy on morphological instability in the freezing of a hypercooled melt. Physica D 161:363–391
11. Hoyle RB, McFadden GB, Davis SH (1996) Pattern selection with anisotropy during directional solidification. Proc R Soc Lond A 354:2915–2949
12. Wu J-B, Bohun CS, Huang H (2008) A thermal elastic model for directional crystal growth with weak anisotropy. SIAM J Appl Math 69(1):283–304
13. Hartman P, Perdok WG (1955) On the relations between structure and morphology of crystals III. Acta Crystallogr 8(9):525–529
14. Li W, Shi E, Chen Z, Yin Z (2000) Growth habit of polar crystals. Chin Sci Bull 45(18):1662–1666
15. Zhong W, Liu G, Shi E (1994) Growth unit and formation mechanisms of crystals under hydrothermal conditions. Sci China B 37(11):1288–1291
16. Zhong W, Tang D (1996) Growth units and morphology of lithium triborate (LBO) crystals. J Cryst Growth 166(1–4):91–98
17. Anslanov LA (1988) Crystal-chemical model of atomic interactions to hexagonal, trigonal and tetragonal systems. Acta Crystallogr B 44(5):458–462
18. Chieh C (1979) The Archimedean truncated octahedron, and packing of geometric units in cubic crystal structures. Acta Crystallogr A 35(6):946–952
19. O'Keeffe M (1978) Non-bonded interactions and the crystal chemistry of tetrahedral structures related to the wurtzite type (B4). Acta Crystallogr B 34(12):3519–3528
20. Parthé E, Engel N (1986) Relation between tetrahedron connections and composition for structures with tetrahedral anion complexes. Acta Crystallogr B 42(6):538–544
21. Parthé E, Chabot B (1990) Classification of structures with anionic tetrahedron complexes using valence-electron criteria. Acta Crystallogr B 46(1):7–23
22. Li W, Shi E, Zhong W, Yin Z (1999) Growth mechanism and growth habit of oxide crystals. J Cryst Growth 203(1–2):186–196
23. Li W, Shi E, Zhong W, Yin Z (1999) Anion coordination polyhedron growth unit: theory, model and crystal morphology. J Synth Cryst 28(2):117–125
24. Li W, Shi E, Chen Z, Yin Z (2001) Coordination polyhedron growth mechanism model and growth habit of crystals. Sci China B 44(2):123–136
25. Yuan R, Shi E, Li W, Zheng Y, Wu N, Zhong W (2000) The growth units and hydrothermal preparation of lead tungstate ($PbWO_4$) crystallites. Sci China E 43(5):495–503
26. Zhang X, Luo H, Zhong W (2004) Growth unit model of anion coordination-polyhedra and its application to crystal growth. Sci China E 47(2):191–202
27. Weiner JH, Boley BA (1963) Elasto-plastic thermal stresses in a solidifying body. J Mech Phys Solids 11:145–154
28. Schwerdtfeger K, Sato M, Tacke K-H (1998) Stress formation in solidifying bodies. Solidification in a round continuous casting mold. Metall Mater Trans B 29:1057–1068

29. Vynnycky M (2009) An asymptotic model for the formation and evolution of air gaps in vertical continuous casting. Proc R Soc A 465:1617–1644
30. Brattkus K, Davis SH (1988) Directional solidification with heat losses. J Cryst Growth 91(4):538–556
31. Hariharan SI, Young GW (2001) Comparison of asymptotic solutions of a phase-field model to a sharp-interface model. SIAM J Appl Math 62(1):244–263
32. Kuiken HK, Roksnoer PJ (1979) Analysis of the temperature distribution in FZ silicon crystals. J Cryst Growth 47(1):29–42
33. Young GW, Chait A (1990) Surface tension driven heat, mass, and momentum transport in a two-dimensional float-zone. J Cryst Growth 106(2–3):445–466
34. Young GW, Heminger JA (1997) Modeling the time-dependent growth of single-crystal fibers. J Cryst Growth 178(3):410–421
35. Young GW, Heminger JA (2000) A mathematical model of the edge-defined film-fed growth process. J Eng Math 38:371–390
36. Liang S (2005) Thermal stress reduction inside InSb crystal grown by Czochralski method. PhD dissertation, York University, Toronto
37. Boley BA, Weiner JH (1997) Theory of thermal stresses, 3rd edn. Dover Publications, New York
38. Mindlin R (1936) Note on the Galerkin and Papkovitch stress functions. Bull Am Math Soc 42:373–376
39. Brantley WA (1973) Calculated elastic constraints for stress problems associated with semiconductor devices. J Appl Phys 44(1):534–535